Spotlight on Applications

Materials Engineering Enabled by Time-Resolved Magneto-Optical Kerr Effect for Spintronic Applications

Dingbin Huang, Dustin Lattery, and Xiaojia Wang*

Cite This: *ACS Appl. Electron. Mater.* 2021, 3, 119−127

Read Online

ACCESS | Metrics & More | Article Recommendations

ABSTRACT: As an updated version of the ultrafast pump−probe laser technique, the time-resolved magneto-optical Kerr effect (TR-MOKE) methodology enables the detection of magnetization dynamics with superb temporal (sub-picosecond) and spatial (diffraction-limited beam spot) resolutions. It is a powerful tool to characterize material properties and to reveal the rich physics of magnetization dynamics in magnetic thin films, which serve as the essential building blocks for spintronic and magnetic recording devices. In this spotlight article, we will highlight the recent advances in the development of TR-MOKE metrology and its applications for capturing the magnetization dynamics in technologically important spintronic materials. We cover several representative examples based on research activities carried out at the University of Minnesota (UMN), including studies of Gilbert damping, spin-strain coupling, and interlayer exchange coupling of perpendicular magnetic materials. A brief discussion will be also presented, which highlights several other emerging research topics that are potentially enabled by this metrology to form a more comprehensive picture of its applications for emerging materials and technologies.

KEYWORDS: ultrafast pump−probe method, time-resolved magneto-optical Kerr effect, perpendicular magnetic anisotropy, damping constant, spintronics
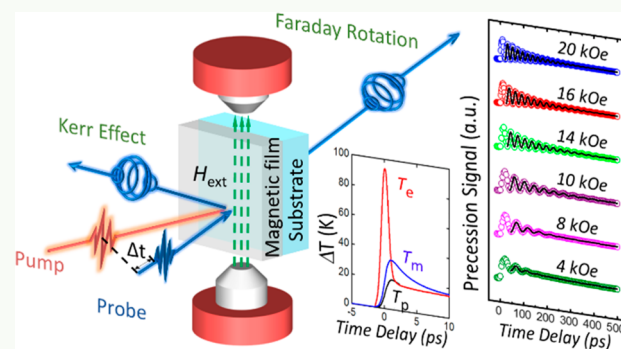
1. INTRODUCTION

Since the discovery of giant magnetoresistance (GMR) in 1988,[1,2] the explosion in spintronics research has led to huge advances in data storage capacity and toward fast, low-power-consumption computers with nonvolatile memory and processing integrated into a single chip. The field of spintronics focuses on utilizing magnetic materials to transport electron angular momentum (spin) instead of the motion of charges (electrons and holes). In principle, manipulating spin would be faster and require less energy (therefore producing less heat load) than moving charges around. Thus, spintronics has been considered a promising candidate to improve, and possibly replace, existing field-effect transistors for processing, transferring, and storing data to achieve the so-called "beyond complementary metal oxide semiconductor (CMOS)" technology.[3]

While spintronic technology has already been proven, materials synthesis and engineering remain as some of the most critical, yet technologically challenging, topics in spintronic research. As an example, spin transfer torque magnetic random-access memory (STT-MRAM) is a typical technology used in spintronic devices. In STT-MRAM, a charge current, which will be polarized after interacting with a magnetic layer (fixed layer), is used to switch the magnet-

ization direction in the free layer and thus to "write" data into the memory. The current required by switching could be described by the critical electronic current density (J_{c0}), which is proportional to the magnetic damping (α, the rate of magnetic energy dissipation).[4] To reduce J_{c0}, and thus the device power consumption, materials with a low α are required. Additionally, a large magnetic anisotropy (K) is preferred for longer data retention times.[4] Furthermore, the existing CMOS manufacturing involves high process temperatures (typically 400 °C).[5] Spintronic materials that can sustain a low α and a high K with post-annealing are favored for the CMOS compatibility. Therefore, developing and engineering magnetic materials with desirable functionalities (e.g., low damping, high anisotropy, and good thermal stability) is essential for device applications.

A better understanding of the material properties and magnetization dynamics can guide the design and synthesis of
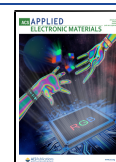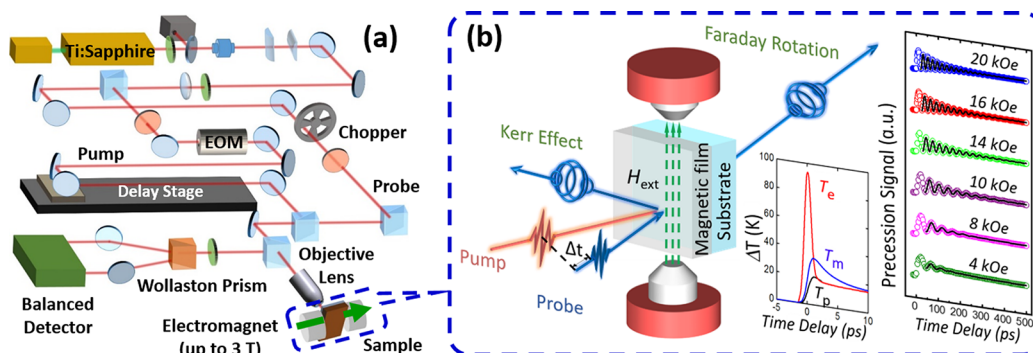
Figure 1. (a) Optical layout of the TR-MOKE system at the UMN. (b) Mechanism of spin dynamics with optical excitation. Both the Kerr effect (reflection) and the Faraday rotation (transmission for (semi)transparent samples) are illustrated, depending on the measurement configuration.
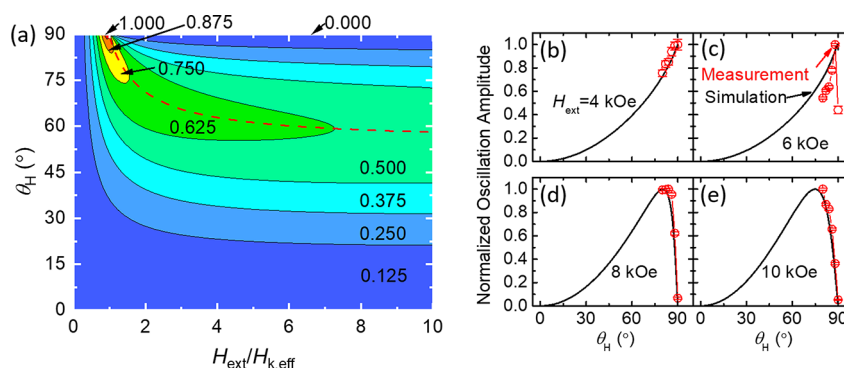

Figure 2. Optimization of TR-MOKE signals. (a) Dependence of the normalized signal amplitude on the normalized external field ($H_{ext}/H_{k,eff}$) and the polar angle of the external field (θ_H). The signal amplitude is normalized such that the maximum possible signal has a value of 1. The dashed red line denotes the maximized signal for a specific field ratio. (b−e) Dependence of normalized signal amplitude on θ_H for different H_{ext} (4, 6, 8, and 10 kOe). Red open circles represent experimental data and black curves are the results from simulations. Figures are reproduced with permission from ref 21. Copyright 2018 AIP Publishing.

materials with desirable functionalities. Conventional approaches for studying the magnetization dynamics and characterizing materials properties are based on ferromagnetic resonance (FMR) techniques. While FMR has adapted some advanced versions (e.g., stripline FMR, among others[6]), it has difficulties characterizing "hard" materials with large perpendicular magnetic anisotropy (PMA) or reaching high dynamic frequencies. Ultrafast optical methods, on the other hand, offer a novel way to inject, detect, and manipulate spin in magnetic materials.[7] Such methods are typically operated in a pump−probe configuration: a pump pulse deposits energy onto the material over a short period of time (<1 ps), and a probe pulse detects the material's response upon the pump excitation. By taking advantage of femtosecond (fs) laser pulses, these ultrafast pump−probe measurements can capture magnetization dynamics at sub-picosecond (sub-ps) resolution, corresponding to a sampling frequency of ∼1 THz. In addition, since the ultrafast pump−probe approach is all-optical, it can probe a localized area of the sample (with diffraction-limited beam spot sizes ranging from micrometers to hundreds of nanometers) instead of measuring the sample-averaged behavior as is done in FMR.

2. INSTRUMENTATION

An upgraded version of the basic pump−probe measurements, the time-resolved magneto-optical Kerr effect (TR-MOKE) methodology enables the detection of magnetization dynamics with superb temporal (sub-ps) and spatial (diffraction-limited beam spot) resolutions.[8−11] At an early stage, TR-MOKE was

used to investigate the ultrafast demagnetization in magnetic materials.[12,13] Later, Ju et al.[14] and Kampen et al.[15] reported the study of magnetization precession based on TR-MOKE measurements. After that, enormous efforts have been devoted to advancing the TR-MOKE methodology, such as interpreting the physical origins of the TR-MOKE signal[10,11,16−20] and optimizing the signal amplitude to improve the measurement signal-to-noise ratio (SNR).[21] To date, TR-MOKE has proven to be a powerful technique which provides sensitive and high-throughput measurements to characterize material properties and to reveal the rich physics of magnetization dynamics of various magnetic materials, which serve as the essential building blocks for spintronic[22] and magnetic recording devices.[23]

Figure 1a depicts the schematics of an example TR-MOKE setup in use at the University of Minnesota (UMN).[8] In TR-MOKE, a mode-locked Ti:sapphire laser produces a train of pulses with a duration of ∼100 fs and a center wavelength of ∼800 nm. A polarizing beam splitter separates the laser into pump and probe beams with orthogonal polarizations. A delay stage varies the optical path of the pump beam, producing a time separation between the pump excitation and probe sensing (up to 4 ns). Both the pump and probe beams are focused onto the sample surface, which produces a beam spot size ($1/e^2$ radius) ranging from hundreds of nanometers to several tens of microns. The reflected probe beam is split into two paths of orthogonal polarizations with a Wollaston prism. The changes in the relative intensities of these two probe paths are detected with a balanced detector, which is related to the
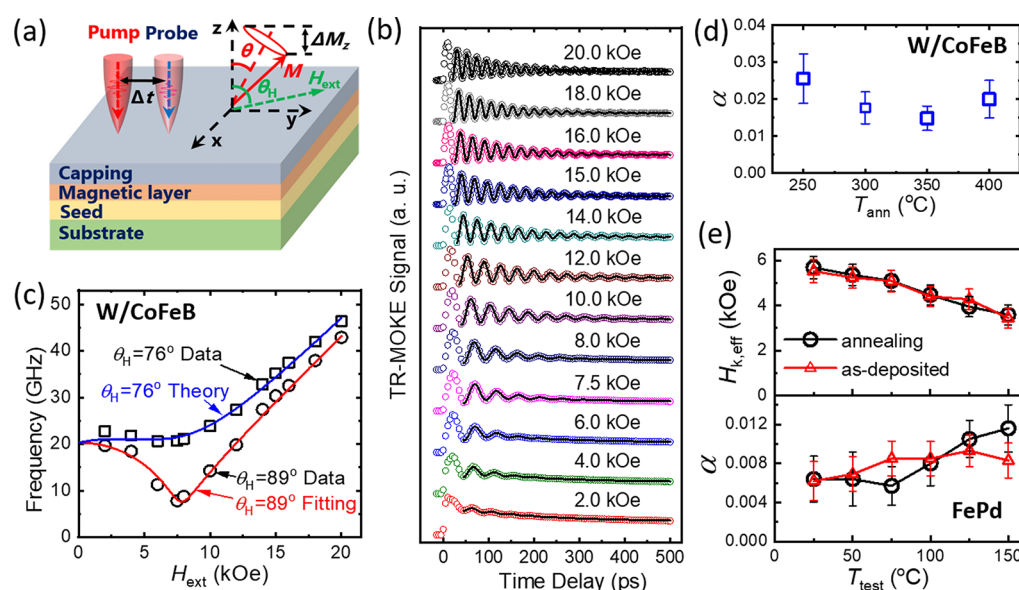
Figure 3. (a) Schematics of the sample stack and measurement configuration. (b) TR-MOKE signals (open circles) and fitting curves (black solid lines) for the 400 °C-annealed CoFeB sample under varying H_{ext} from 2.0 to 20 kOe at $\theta_H = 76°$. (c) The fitting of f vs H_{ext} for the 400 °C-annealed CoFeB sample at two field directions. Measurement data are shown as symbols (open circles for $\theta_H = 89°$ and open squares for $\theta_H = 76°$), and model fittings are presented as solid curves. (d) The damping constant of CoFeB samples as a function of T_{ann}. (e) The dependence of $H_{k,eff}$ (top) and α (bottom) on the test temperature, T_{test}, for as-deposited and 400 °C-annealed FePd films. Figures are reproduced with permissions from refs 26 and 27. Copyright 2018 Springer and 2020 AIP Publishing.

variations in the polarization state of the probe beam reflected from the magnetic sample. On the basis of the probe polarization variation, the change in the sample magnetization can be correlated to the Kerr rotation angle via the MOKE effect.[24] At short time delays ($\Delta t < 10$ ps, the time between pump heating and probe sensing), the TR-MOKE signal is dominated by the thermalization processes between different energy carriers, namely, electrons, magnons (quantized states of spin waves), and phonons (quantized states of lattice waves). Within this nonequilibrium regime, TR-MOKE signals can be analyzed by a phenomenological three-temperature model that considers energy exchange between electrons (T_e), phonons (T_p), and magnons (T_m).[12] At longer time delays (hundreds of ps), TR-MOKE signals contain damped oscillating fringes resulting from spin precession, which allows for the analysis of the damping constant of magnetic materials (see Figure 1b).[8] In addition to TR-MOKE, pump–probe measurements can also be conducted in other modes. For (semi)transparent samples, the pump–probe measurements can also be operated in the transmission mode to collect the Faraday rotation signals.

For TR-MOKE measurements, the signal amplitude is crucial since it can affect the measurement SNRs and thus the accuracy and reliability of the measurement results, especially for measuring samples with large effective damping. To better understand how measurement conditions could affect the signal amplitudes, Lattery et al.[21] systematically studied the impact of the direction and amplitude of the external field on the TR-MOKE signal amplitude. They simulated the time-resolved signals and compared these calculated values with measurement results of a PMA CoFeB thin film obtained from polar TR-MOKE (the signal is proportional to the change of the magnetization along the sample normal direction).[9] Their major discoveries are shown in Figure 2a as a contour plot, which illustrates the dependence of the TR-MOKE signal on the direction (as indicated by θ_H, the angle between the

external field and the sample surface normal) and magnitude (H_{ext}) of the external field. The horizontal axis is normalized to the effective anisotropy field ($H_{k,eff}$) of the sample to generalize the application of the results. For small external fields ($H_{ext}/H_{k,eff} < 1$), the signal amplitude increases with θ_H. While for large external fields ($H_{ext}/H_{k,eff} > 1$), there exists a θ_H at which the signal amplitude is maximized for each individual field, as indicated by the red dashed line in Figure 2a. This contour can be used to guide the choice of measurement conditions for signal optimization. For example, if the sample will be measured with varying external fields of up to $H_{ext}/H_{k,eff} = 2$ and a fixed θ_H, then the field direction that generates the maximal signals should be larger than 70°. For measurements where H_{ext} is fixed and θ_H is varied, the optimal field generating the maximal signal amplitude is not necessarily at the largest H_{ext}.

Figure 2b–e summarizes the experimental validation of the simulation results. The PMA CoFeB thin film ($H_{k,eff} = 6.1$ kOe) was measured at varying θ_H for four sets of fixed H_{ext} (4, 6, 8, and 10 kOe). Because of the design of measurement configuration, the range of θ_H was confined from 80° to 90°. Within this range of θ_H, the amplitudes from TR-MOKE signals (red symbols) match well with simulation results (solid curves). For the 4-kOe case ($H_{ext} < H_{k,eff}$), the signal amplitude increases monotonically with θ_H, while for the 8-kOe and 10-kOe cases ($H_{ext} > H_{k,eff}$), the signal amplitude shows a peak at the predicted optimal θ_H. For the 6-kOe case where H_{ext} is close to $H_{k,eff}$, there is a slight deviation in the decaying trend of the signal amplitude for decreasing θ_H (a slower decrease trend from simulations). A possible explanation is the sample has inhomogeneity in $H_{k,eff}$, which can result in a noticeable deviation from simulations when H_{ext} is close to $H_{k,eff}$. However, the measurement can still capture the amplitude peak occurring at nearly the same θ_H (close to 90°) from model prediction as shown in Figure 2c.

3. REPRESENTATIVE EXAMPLES

We will now show in detail the applications of the TR-MOKE metrology by presenting representative examples, primarily based on the studies conducted by the authors' group at the UMN. These examples include measuring the Gilbert damping constant of PMA magnetic thin films, revealing the spin-strain coupling in multilayer stacks, and exploring interlayer exchange coupling in synthetic antiferromagnetic materials.

3.1. Gilbert Damping. The Gilbert damping constant (α) is related to how fast the magnetization relaxes to equilibrium[25] and therefore is a critical parameter for the performance of spintronic devices. As mentioned in the introduction, a low α is preferred in the free layer for STT-MRAM applications because it can reduce the switching current.[4] The dependence of α on various factors, such as material compositions, stack structures, and fabrication processes, has been stimulating progressively more interest in the spintronics community. These studies rely on the accurate characterization of α. After more than 10 years of advancement in measuring and modeling, TR-MOKE has been proven to be a reliable way to extract α for a wide range of materials.[20] Also, since TR-MOKE can capture high resonance frequencies that conventional FMR may fail to detect, it has become a popular approach when dealing with PMA materials that may have a relatively high anisotropy.[20] For damping measurements enabled by TR-MOKE, we will use two representative PMA materials as illustrations: CoFeB with interfacial anisotropy[26] and $L1_0$-FePd with crystalline anisotropy,[27] both of which have technological relevance.

CoFeB is currently one of the most widely applied PMA materials in magnetic tunnel junctions (MTJs), a basic component of spintronic devices. For MTJs-based device applications, an ideal spintronic material is preferred to have both low damping and high effective anisotropy. In addition, for integration with current CMOS technologies, the materials are required to survive through a processing temperature of up to 400 °C.[5] For this purpose, Lattery et al. studied the dependence of α on the post-annealing temperature (T_{ann}) present during the fabrication of CoFeB thin films with interfacial PMA.[26] They fabricated a set of sample stacks consisting of $Si/SiO_2(300)/W(7)/CoFeB(1.2)/MgO(2)/Ta(3)$ from bottom to top (thicknesses in nanometers) and annealed those samples at T_{ann} ranging from 250 to 400 °C. Tungsten (W) was used as the seed layer in this study, owing to the relatively smaller diffusion of W atoms compared with Ta, another popular seed material for PMA CoFeB. By utilizing the polar TR-MOKE metrology described in section 2, Lattery et al. measured these W-seeded CoFeB samples under different external magnetic fields. The signal directly taken from polar TR-MOKE is the change in the z-component of the magnetization (ΔM_z in Figure 3a), which is proportional to the change of the Kerr rotation angle ($\Delta\theta_K$). Figure 3b depicts the raw data (open circles) as a function of the time delay between pump excitation and probe sensing for H_{ext} ranging from 2 to 20 kOe. All signals show a damped oscillating feature and can be fitted using the equation $\Delta\theta_K = A + Be^{-t/C} + D\sin(2\pi ft + \varphi)e^{-t/\tau}$. The first two terms in the equation are related to the thermal background. The last term, an exponentially decaying sinusoidal function, incorporates the frequency (f) and relaxation time (τ, used for the determination of damping) of the spin precession.

The data reduction of spin precessional signals for a magnetic material mainly includes the analyses of precessional frequency and the relaxation time. The precessional frequency can be well described by the Kittel formula for different sample shapes and certain orientations of the external field.[28] For a more generalized analysis, the Smit-Suhl approach can predict the precessional frequency based on the magnetic free energy.[29] With the known measurement parameters (θ_H and the magnitude of H_{ext}), the fitting of f vs H_{ext} gives the anisotropic field ($H_{k,eff}$) and the gyromagnetic ratio (γ) of the sample. Once $H_{k,eff}$ is known, the "intrinsic" Gilbert damping (α) can be determined from the fitting of the relaxation time, τ, measured by TR-MOKE. The value of τ from TR-MOKE can be related to the "effective" damping via $\alpha_{eff} = 1/2\pi f\tau$. α_{eff} is dependent on the measurement conditions (e.g., θ_H and the magnitude of H_{ext}) and contains contributions from both the intrinsic Gilbert damping and inhomogeneous broadening. Ideally, one would conduct measurements at sufficiently high fields ($H_{ext} \gg H_{k,eff}$) to suppress inhomogeneous broadening, such that α_{eff} is approximately the same as α. More practically, the inhomogeneity contribution can be removed from α_{eff} based on model analysis, as has been demonstrated by several research groups.[10,19,20,26] It should be noted here that most of the model predictions of α typically start with the Landau–Lifshitz–Gilbert (LLG) equation. For measurements taken at elevated temperatures close to T_C (Curie temperature), however, the Landau–Lifshitz–Bloch (LLB) theory is more appropriate to be used for data reduction.[30−32] The use of the LLB theory is necessary when studying media materials used for heat-assisted magnetic recording.

Figure 3c shows the frequency fitting of the CoFeB sample annealed at 400 °C for two field directions ($\theta_H = 76°$ and 89°). For the data taken at 89° (close to the in-plane direction), the frequency shows a dip at $H_{ext} \approx H_{k,eff}$ resulting from the difficulty in initiating the precession at this H_{ext}, where the Zeeman energy balances out the rest of the energy terms. This dip feature diminishes when θ_H decreases to 76°. For both cases, the model agrees well with measurement results. Figure 3d summarizes the α values of CoFeB samples annealed at different temperatures. α decreases with T_{ann} at first, until it reaches its minimum (0.015) at T_{ann} = 350 °C, and then it increases with T_{ann}. Two competing effects are used to explain this trend: the crystallization of CoFeB and the dead-layer growth at the interfaces of the CoFeB film, both of which are more pronounced at elevated T_{ann}. The crystallization tends to reduce α, while the dead-layer formation increases α, leading to the minimal α when the CoFeB sample is annealed at 350 °C. Overall, α remains low (0.015−0.025) for T_{ann} up to 400 °C, which suggests W-seeded CoFeB thin films have high thermal stability and thus good compatibility with the CMOS fabrication process.

The second representative material, $L1_0$-FePd, is also favored in MTJ applications owing to its high crystalline anisotropy and low α. Since the operating temperature of spintronic devices can also vary (e.g., −55 to 150 °C),[33] the dependence of α on the operating temperature, in addition to T_{ann} during fabrication processes, is also critical for device performance. For this purpose, Zhang et al. synthesized Ru-seeded $L1_0$-FePd thin films that were both as-deposited and annealed at 400 °C.[27] They then studied the damping constant of those $L1_0$-FePd thin films using TR-MOKE, at the test temperature (T_{test}) ranging from room temperature (RT) to 150 °C (as the upper limit of device operating temperature).

Figure 3e summarizes the T_{test}-dependence of $H_{k,eff}$ and α obtained from TR-MOKE. When T_{test} changes from RT to 150 °C, $H_{k,eff}$ decreases from ~5.7 kOe to ~3.6 kOe for both samples, while α slightly increases with T_{test} (from 0.006 to 0.009 for as-deposited FePd and from 0.006 to 0.012 for 400 °C-annealed FePd). Overall, both samples sustain a small α (≤ 0.012) for T_{test} up to 150 °C, suggesting the Ru-seeded $L1_0$-phase FePd films possess high thermal stability for both fabrication and operation processes.

3.2. Spin-Strain Coupling. The coupling between spin and strain enables strain-assisted manipulation of magnetization with less energy consumption.[34] Because of this, the area of "straintronics of magnetic materials" has been drawing more and more attention for developing energy-saving technologies in spintronics. Most of the previous efforts have been devoted to the electrical generation of surface acoustic waves (SAWs) using piezoelectric materials, which induces strain into the magnetic layer.[35] However, the strain frequency generated with electrical approaches is relatively low compared with that from optical excitation. In addition, most of the materials studied in the literature (e.g., Ni,[36,37] Bi-YIG,[38] Terfenol-D,[39] and Gafenol[40]) are not suitable for practical spintronic applications, resulting from their low resonant frequency, low anisotropy, or low T_C.

To address these issues, Zhang et al. conducted TR-MOKE measurements on PMA $[Co/Pd]_n$ multilayers to explore the coupling mechanisms between spin (magnon) and strain (phonon).[41] The sample stack information and measurement configuration are illustrated in Figure 4a. Upon optical excitation, both strain (via thermal expansion) and spin (via thermal demagnetization) can be launched, simultaneously, within the magnetic layer. The strain frequency is related to the longitudinal acoustic wave propagation and is tunable by varying the sample film thickness. For films with thicknesses on the order of nanometers, the strain frequency can reach tens or hundreds of GHz, beyond what is practical with electrical approaches. Another advantage of TR-MOKE is the high temporal resolution resulting from fs laser pulses, which enables the detection of dynamics at extremely high frequencies. The $[Co/Pd]_n$ multilayers were chosen as the material system in this study, because $[Co/Pd]_n$ multilayers have high a RT PMA and a relatively large magnetostriction coefficient ($\lambda \approx -1 \times 10^{-4}$),[42,43] favored for practical applications.

Figure 4b depicts the TR-MOKE signals for the $[Co/Pd]_n$ multilayer as a function of time delay under varying H_{ext} from 10−29 kOe. The thickness of this multilayer was optimized such that the spin-strain coupling could be observed within the available field range (up to 30 kOe). In contrast with the monotonic decaying trend of the oscillation amplitude for CoFeB (Figure 3b), the oscillation amplitude of $[Co/Pd]_n$ increases in the first 60 ps after the pump excitation and then shows the usual damped feature. This leads to a magneto-acoustic resonance region when H_{ext} changes from 18 to 24 kOe. Within this resonance region, the spin-strain coupling is more effective, enabling the energy flow from strain to the spin system to overcome the energy dissipation (due to the damping) in the magnetic material system. Directly from measurements, TR-MOKE signals contain two modes with different frequencies, as can be seen from the fast Fourier transfer (FFT) of TR-MOKE signals shown in Figure 4c. Outside of the resonance region, one mode is driven by magnons (FMR mode), and the other mode is driven by phonons (strain mode). The two modes are separated from each other (H_{ext} = 14 kOe). Within the resonance region, the FMR and strain modes are hybridized, and the two peaks are overlapping for the 21 kOe case.

The magneto-acoustic resonance can be better visualized in the field-dependent plots of the frequency and amplitude of the precessional signals, as shown in Figure 5a,b. There are two modes observable over the entire field range, which are defined as the low-frequency (LF) mode (black circles) and the high-frequency (HF) mode (red diamonds). Within the resonance region (highlighted in light blue), the frequencies of these two modes approach each other and show an anticrossing feature. For fields lower than the resonance region, the LF mode is mainly attributed to the contributions from magnons (FMR mode), whereas the HF mode is dominated by the contributions from phonons (strain mode). At fields higher than the resonance region, the mode contributions are reversed. The frequencies of the strain mode are field independent, while the frequencies of the FMR mode follow the typical linear dependence on H_{ext} (guided by the blue dashed line). The magneto-acoustic resonance frequency is ~60 GHz at 21 kOe, which is predetermined by the frequencies of the strain mode. This is, by far, the highest magneto-acoustic resonance frequency observed in experiments. The spin-strain coupling is also reflected by a local maximum in the amplitude plot within the resonance region. Furthermore, a theoretical model was proposed to explain the coupling mechanisms, which gives a coupling coefficient of 272 GHz.[2] This study of spin-strain coupling, enabled by TR-MOKE, is the first experimental demonstration of extremely high-frequency magneto-acoustic resonance. It opens the possibility of utilizing spin-strain coupling to achieve ultra-high-speed magnetization switching.
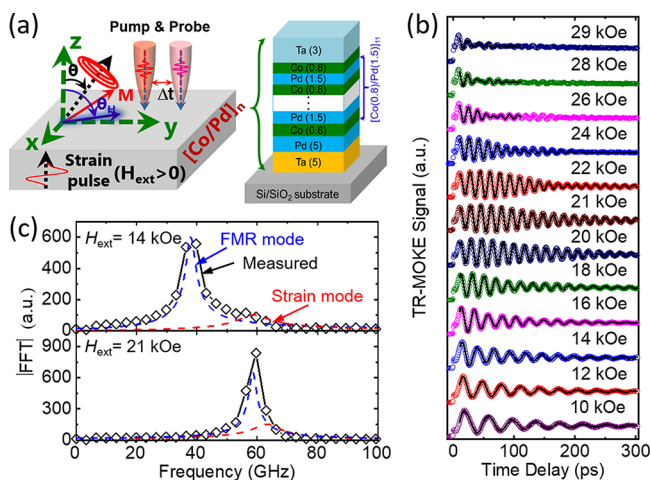

Figure 4. (a) Schematics of the sample system under H_{ext} and the excitation of laser pulses. Upon the excitation of the pump pulse, both magnetization precession and strain will be launched in the sample stack. (b) TR-MOKE signals (symbols) and model fitting (curves) for the $[Co/Pd]_n$ multilayer under varying H_{ext} at θ_H = 80°. The amplitude of precession increases with the time delay for 18 kOe < H_{ext} < 24 kOe. (c) The fast Fourier transfer (FFT) of measured time-domain signals for the case of H_{ext} = 14 kOe (top) and 21 kOe (bottom). The frequency spectra consist of two peaks, which are separate at 14 kOe and overlapping at 21 kOe. Figures are reproduced with permission from ref 41. Copyright 2020 AAAS.
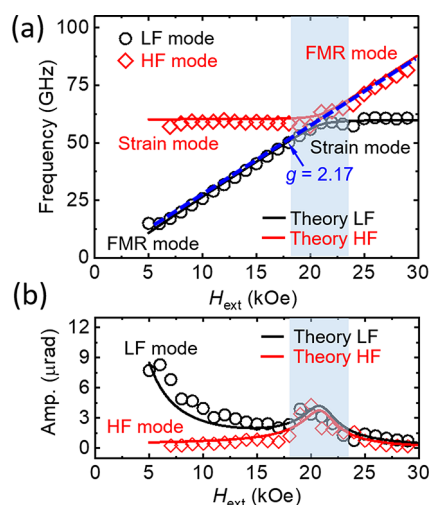
Figure 5. Field-dependent plots of oscillation frequency (a) and amplitude (b). Within the magneto-acoustic resonance region (highlighted in blue), the frequencies of the HF and LF modes show an anticrossing feature, and the amplitudes increase for both modes. The linear dependence of f vs H_{ext} for the magnon-driven FMR mode results in a value of 2.17 for the g factor of the measured $[Co/Pd]_n$ multilayer. For both panels, open symbols represent experimental data, and solid curves denote the model calculation. Figures are reproduced with permission from ref 41. Copyright 2020 AAAS.

3.3. Synthetic Antiferromagnetic (SAF) Structures.

Synthetic antiferromagnetic (SAF) materials involve more complex sample structures. As shown in Figure 6, a typical SAF
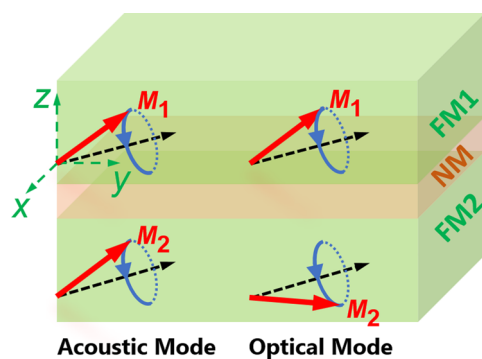

Figure 6. Schematic of a nominal SAF structure, where two ferromagnetic layers (FM1 and FM2) are separated by a nonmagnetic layer (NM). Two precession modes, namely, acoustic mode and optical mode, are also illustrated at sufficiently high external fields (Zeeman energy dominants). For the acoustic (optical) mode, M_1 and M_2 precess in-phase (out-of-phase) around their individual equilibrium directions, as denoted by the black dashed arrows.

structure consists of two ferromagnetic (FM) layers separated by a nonmagnetic (NM) layer. These two FM layers are exchange-coupled with individual magnetizations aligned antiparallelly through the Ruderman−Kittel−Kasuya−Yosida (RKKY) interaction.[44,45] SAF structures have low stray fields, high stability when exposed to external fields, and extra flexibilities to tune their magnetic properties.[46,47] Therefore, SAF materials have been proposed as promising building elements in MTJs,[46−48] spin oscillators,[49] and magnonic devices.[50] For SAF, both the damping and the interlayer

coupling strength are important properties that affect the dynamics of the system. Such properties have been successfully characterized by FMR in the literature; however, most of the SAF structures studied by FMR possess an in-plane magnetic anisotropy (IMA-SAF).[5,51−53] Very recently, TR-MOKE has extended the dynamic studies of SAF structures to cover both IMA-SAF and PMA-SAF materials,[54−56] owing to its capabilities of reaching high precessional frequencies and large external fields.[20,57,58]

Similar to the spin-strain coupling introduced in section 3.2, the coupling between two FM layers can also lead to two modes, the HF mode and the LF mode, with different frequency dependence on H_{ext}. The data taken at low fields are more challenging to interpret due to the complex magnetization behavior and a larger contribution from inhomogeneous broadening; therefore, the high-field data are used to elucidate the magnetization dynamics. In the high-field region, the Zeeman energy dominates, and thus the equilibrium directions of the magnetizations (M_1 and M_2) for the two FM layers are almost parallel with the external field. In this region, the HF mode corresponds to the "acoustic mode" where M_1 and M_2 precess in-phase, and the LF mode corresponds to the "optical mode" with out-of-phase precession of M_1 and M_2, as illustrated in Figure 6. Since the directions of M_1 and M_2 are aligned parallelly with the external field and change little with the field strength, there is a nearly linear field dependence of the frequencies for both the HF and LF modes at sufficiently high fields. The dependence of f vs H_{ext} can be well described by a theoretical model which considers the coupling strength between two layers.[59,60] The exchange field (H_{ex}) can be extracted from the model fitting of frequency data in the high-field region.[61] To date, the damping studies using TR-MOKE for PMA-SAF structures are still limited in scope, and only the effective damping constant has been reported in the literature.[55,56] A comprehensive model for separating the intrinsic α from the inhomogeneous broadening contribution is still missing and needs further development.

4. ADDITIONAL EMERGING RESEARCH TOPICS ENABLED BY TR-MOKE

Besides the research topics discussed above, TR-MOKE has also been utilized to explore several other emerging topics in the spintronic community. One example involves the use of TR-MOKE to study the spin−orbital torque (SOT) effect, which provides a promising switching mechanism for MRAM applications.[61] Because of spin−orbital coupling, a charge current can generate both field-like torque and damping-like torque in magnetic materials, and thus, it can modulate the magnetization dynamics. TR-MOKE can detect the impact of charge current on the damping constant, allowing the study of the SOT effect.[61] Another example is the characterization of spin current transfer efficiency across interfaces using TR-MOKE. This was demonstrated in a recent work by Panda et al., who investigated the interfacial spin transparency of a β-Ta/CoFeB structure by measuring the thickness-dependent Gilbert damping.[62]

In addition to spintronics, TR-MOKE has also enabled the study of spin-wave generation and detection in magnetic materials with superb temporal and spatial resolutions. This is of technological importance in the field of magnonics for developing low-energy-dissipation devices.[63] One example is an all-optical study of coherent spin-wave generation in a permalloy thin film conducted by Iihama et al., where they

performed 2D scanning TR-MOKE measurements to detect the propagation of spin-wave packets excited by ultrafast laser pulses.[64]

In a broader picture, the TR-MOKE metrology can also be applied for studying other transport properties of materials, such as the thermal conductivity and interfacial thermal conductance of the materials. For thermal transport studies, the basic pump−probe mode of time-domain thermoreflectance (TDTR) is typically used. TDTR interrogates the temperature-dependent reflectivity of the probe beam reflected from the sample surface upon pump heating and subsequent cooling. Compared with TDTR, TR-MOKE offers improved sensitivities for thermal property measurements, especially for materials with in-plane thermal anisotropy. This is mainly attributed to the use of an optically thin magnetic transducer with a relatively low thermal conductivity in TR-MOKE, which minimizes the in-plane thermal transport in the magnetic transducer and thus enhances the measurement sensitivity to the in-plane thermal properties of the underlying materials.[8,65−68] Furthermore, as mentioned in section 2, the short time-delay TR-MOKE signal is dominated by the thermalization processes between different energy carriers (electrons, magnons, and phonons). By analyzing TR-MOKE data taken within this nonequilibrium regime, the coupling between different energy carriers can be understood. Such an understanding can provide insight into the ultrafast demagnetization process, which is important for maximizing the TR-MOKE signal, exploring thermally induced spin current generation and enhancing the efficiency of all-optical magnetic switching.[69,70]

5. SUMMARY

In this spotlight article, the TR-MOKE metrology is highlighted as an enabling technique to study a wide range of magnetic materials for spintronic applications. Since TR-MOKE combines the advantages of fs-optical excitation/detection, and diffraction limited areas for probing, it can offer superb temporal (sub-ps) and spatial (micrometers to hundreds of nanometers) resolutions. A number of example applications of TR-MOKE are discussed, including experimental studies of the damping constant of PMA thin films, the spin-strain coupling in PMA multilayers, and the magnetization dynamics of PMA-SAF structures, exceeding the capabilities of conventional approaches. As a powerful tool, TR-MOKE has enabled new research of physical phenomena, including the SOT effect, spin wave detection, thermally induced spin current generation, and ultrafast energy carrier coupling. Its applications can even be extended to the study of thermal transport in materials. The rich physics and mechanisms revealed by TR-MOKE will in turn guide the design and engineering of materials with desirable functionalities for high-performance devices.

■ AUTHOR INFORMATION

Corresponding Author

Xiaojia Wang − *Department of Mechanical Engineering, University of Minnesota, Minneapolis, Minnesota 55455, United States;* ● orcid.org/0000-0001-7612-1739; Email: wang4940@umn.edu

Authors

Dingbin Huang − *Department of Mechanical Engineering, University of Minnesota, Minneapolis, Minnesota 55455, United States;* ● orcid.org/0000-0001-8648-9801

Dustin Lattery − *Department of Mechanical Engineering, University of Minnesota, Minneapolis, Minnesota 55455, United States;* ● orcid.org/0000-0002-3614-4677

Complete contact information is available at:
https://pubs.acs.org/10.1021/acsaelm.0c00961

Notes

The authors declare no competing financial interest.

■ ACKNOWLEDGMENTS

■ REFERENCES

(1) Baibich, M. N.; Broto, J. M.; Fert, A.; Van Dau, F. N.; Petroff, F.; Etienne, P.; Creuzet, G.; Friederich, A.; Chazelas, J. Giant Magnetoresistance of (001)Fe/(001)Cr Magnetic Superlattices. *Phys. Rev. Lett.* **1988**, *61* (21), 2472−2475.

(2) Binasch, G.; Grünberg, P.; Saurenbach, F.; Zinn, W. Enhanced Magnetoresistance in Layered Magnetic Structures with Antiferromagnetic Interlayer Exchange. *Phys. Rev. B: Condens. Matter Mater. Phys.* **1989**, *39* (7), 4828−4830.

(3) Wolf, S. A.; Awschalom, D. D.; Buhrman, R. A.; Daughton, J. M.; von Molnár, S.; Roukes, M. L.; Chtchelkanova, A. Y.; Treger, D. M. Spintronics: A Spin-Based Electronics Vision for the Future. *Science* **2001**, *294* (5546), 1488−1495.

(4) Chun, K. C.; Zhao, H.; Harms, J. D.; Kim, T. H.; Wang, J. P.; Kim, C. H. A scaling Roadmap and Performance Evaluation of In-Plane and Perpendicular MTJ Based STT-MRAMs for High-Density Cache Memory. *IEEE J. Solid-State Circuits* **2013**, *48* (2), 598−610.

(5) Annunziata, A. J.; Trouilloud, P. L.; Bandiera, S.; Brown, S. L.; Gapihan, E.; O'Sullivan, E. J.; Worledge, D. C. Materials Investigation for Thermally-Assisted Magnetic Random Access Memory Robust Against 400°C Temperatures. *J. Appl. Phys.* **2015**, *117*, No. 17B739.

(6) Farle, M.; Silva, T.; Woltersdorf, G. Spin Dynamics in the Time and Frequency Domain. In *Magnetic Nanostructures: Spin Dynamics and Spin Transport*; Zabel, H.; Farle, M., Eds.; Springer: Berlin, Heidelberg, 2013; pp 37−83.

(7) Kirilyuk, A.; Kimel, A. V.; Rasing, T. Ultrafast Optical Manipulation of Magnetic Order. *Rev. Mod. Phys.* **2010**, *82* (3), 2731−2784.

(8) Zhu, J.; Wu, X.; Lattery, D. M.; Zheng, W.; Wang, X. The Ultrafast Laser Pump-Probe Technique for Thermal Characterization of Materials With Micro/Nanostructures. *Nanoscale Microscale Thermophys. Eng.* **2017**, *21* (3), 177−198.

(9) Lattery, D. M.; Zhu, J.; Huang, D.; Wang, X. Ultrafast Thermal and Magnetic Characterization of Materials Enabled by the Time-Resolved Magneto-Optical Kerr Effect. In *Nanoscale Energy Transport*; Liao, B., Ed.; IOP Publishing, 2020; pp 9−30.

(10) Iihama, S.; Mizukami, S.; Naganuma, H.; Oogane, M.; Ando, Y.; Miyazaki, T. Gilbert Damping Constants of Ta/CoFeB/MgO(Ta) Thin Films Measured by Optical Detection of Precessional Magnetization Dynamics. *Phys. Rev. B: Condens. Matter Mater. Phys.* **2014**, *89*, 174416.

(11) Mizukami, S. Fast Magnetization Precession and Damping for Magnetic Films with High Perpendicular Magnetic Anisotropy. *J. Magn. Soc. Jpn.* **2015**, *39* (1), 1−7.

(12) Beaurepaire, E.; Merle, J.-C.; Daunois, A.; Bigot, J.-Y. Ultrafast Spin Dynamics in Ferromagnetic Nickel. *Phys. Rev. Lett.* **1996**, *76*, 4250.

(13) Ju, G.; Vertikov, A.; Nurmikko, A. V.; Canady, C.; Xiao, G.; Farrow, R. F. C.; Cebollada, A. Ultrafast Nonequilibrium Spin Dynamics in a Ferromagnetic Thin Film. *Phys. Rev. B: Condens. Matter Mater. Phys.* **1998**, *57* (2), R700−R703.

(14) Ju, G.; Nurmikko, A. V.; Farrow, R. F. C.; Marks, R. F.; Carey, M. J.; Gurney, B. A. Ultrafast Time Resolved Photoinduced Magnetization Rotation in a Ferromagnetic/Antiferromagnetic Exchange Coupled System. *Phys. Rev. Lett.* **1999**, *82* (18), 3705−3708.

(15) van Kampen, M.; Jozsa, C.; Kohlhepp, J. T.; LeClair, P.; Lagae, L.; de Jonge, W. J. M.; Koopmans, B. All-Optical Probe of Coherent Spin Waves. *Phys. Rev. Lett.* **2002**, *88* (22), 227201.

(16) Barman, A.; Wang, S.; Hellwig, O.; Berger, A.; Fullerton, E. E.; Schmidt, H. Ultrafast Magnetization Dynamics in High Perpendicular Anisotropy [Co/Pt]$_n$ Multilayers. *J. Appl. Phys.* **2007**, *101*, No. 09d102.

(17) Mizukami, S.; Sajitha, E. P.; Watanabe, D.; Wu, F.; Miyazaki, T.; Naganuma, H.; Oogane, M.; Ando, Y. Gilbert Damping in Perpendicularly Magnetized Pt/Co/Pt Films Investigated by All-Optical Pump-Probe Technique. *Appl. Phys. Lett.* **2010**, *96*, 152502.

(18) Iihama, S.; Ma, Q.; Kubota, T.; Mizukami, S.; Ando, Y.; Miyazaki, T. Damping of Magnetization Precession in Perpendicularly Magnetized CoFeB Alloy Thin Films. *Appl. Phys. Express* **2012**, *5* (8), 083001.

(19) Iihama, S.; Sakuma, A.; Naganuma, H.; Oogane, M.; Mizukami, S.; Ando, Y. Influence of L1$_0$ Order Parameter on Gilbert Damping Constants for FePd Thin Films Investigated by Means of Time-Resolved Magneto-Optical Kerr Effect. *Phys. Rev. B: Condens. Matter Mater. Phys.* **2016**, *94*, 174425.

(20) Capua, A.; Yang, S. H.; Phung, T.; Parkin, S. S. P. Determination of Intrinsic Damping of Perpendicularly Magnetized Ultrathin Films From Time-Resolved Precessional Magnetization Measurements. *Phys. Rev. B: Condens. Matter Mater. Phys.* **2015**, *92*, 224402.

(21) Lattery, D. M.; Zhu, J.; Zhang, D.; Wang, J. P.; Crowell, P. A.; Wang, X. Quantitative Analysis and Optimization of Magnetization Precession Initiated by Ultrafast Optical Pulses. *Appl. Phys. Lett.* **2018**, *113* (16), 162405.

(22) Yu, G. Two-terminal MRAM with a spin. *Nat. Electron.* **2018**, *1*, 496−497.

(23) Muthsam, O.; Slanovc, F.; Vogler, C.; Suess, D. The Superior Role of the Gilbert Damping on the Signal-to-Noise Ratio in Heat-Assisted Magnetic Recording. *J. Magn. Magn. Mater.* **2020**, *514*, 167125.

(24) You, C. Y.; Shin, S. C. Generalized Analytic Formulae for Magneto-Optical Kerr Effects. *J. Appl. Phys.* **1998**, *84* (1), 541−546.

(25) Hickey, M. C.; Moodera, J. S. Origin of Intrinsic Gilbert Damping. *Phys. Rev. Lett.* **2009**, *102* (13), 137601.

(26) Lattery, D. M.; Zhang, D.; Zhu, J.; Hang, X.; Wang, J. P.; Wang, X. Low Gilbert Damping Constant in Perpendicularly Magnetized W/CoFeB/MgO Films with High Thermal Stability. *Sci. Rep.* **2018**, *8*, 13395.

(27) Zhang, D.; Huang, D.; Wu, R. J.; Lattery, D.; Liu, J.; Wang, X.; Gopman, D. B.; Mkhoyan, K. A.; Wang, J. P.; Wang, X. Low Gilbert Damping and High Thermal Stability of Ru-Seeded L1$_0$-Phase FePd Perpendicular Magnetic Thin Films at Elevated Temperatures. *Appl. Phys. Lett.* **2020**, *117* (8), 082405.

(28) Kittel, C. On the Theory of Ferromagnetic Resonance Absorption. *Phys. Rev.* **1948**, *73* (2), 155−161.

(29) Suhl, H. Ferromagnetic Resonance in Nickel Ferrite Between One and Two Kilomegacycles. *Phys. Rev.* **1955**, *97* (2), 555−557.

(30) Evans, R. F. L.; Hinzke, D.; Atxitia, U.; Nowak, U.; Chantrell, R. W.; Chubykalo-Fesenko, O. Stochastic Form of the Landau-Lifshitz-Bloch Equation. *Phys. Rev. B: Condens. Matter Mater. Phys.* **2012**, *85* (1), 014433.

(31) Ostler, T. A.; Ellis, M. O. A.; Hinzke, D.; Nowak, U. Temperature-Dependent Ferromagnetic Resonance via the Landau-Lifshitz-Bloch Equation: Application to FePt. *Phys. Rev. B: Condens. Matter Mater. Phys.* **2014**, *90* (9), 094402.

(32) Strungaru, M.; Ruta, S.; Evans, R. F. L.; Chantrell, R. W. Model of Magnetic Damping and Anisotropy at Elevated Temperatures: Application to Granular FePt Films. *Phys. Rev. Appl.* **2020**, *14* (1), 014077.

(33) Iwata-Harms, J. M.; Jan, G.; Liu, H.; Serrano-Guisan, S.; Zhu, J.; Thomas, L.; Tong, R. Y.; Sundar, V.; Wang, P. K. High-Temperature Thermal Stability Driven by Magnetization Dilution in CoFeB Free Layers for Spin-Transfer-Torque Magnetic Random Access Memory. *Sci. Rep.* **2018**, *8*, 14409.

(34) Biswas, A. K.; Bandyopadhyay, S.; Atulasimha, J. Acoustically Assisted Spin-Transfer-Torque Switching of Nanomagnets: An Energy-Efficient Hybrid Writing Scheme for Non- Volatile Memory. *Appl. Phys. Lett.* **2013**, *103*, 232401.

(35) Thevenard, L.; Camara, I. S.; Majrab, S.; Bernard, M.; Rovillain, P.; Lemaître, A.; Gourdon, C.; Duquesne, J. Y. Precessional Magnetization Switching by a Surface Acoustic Wave. *Phys. Rev. B: Condens. Matter Mater. Phys.* **2016**, *93* (13), 134430.

(36) Kim, J. W.; Vomir, M.; Bigot, J. Y. Ultrafast Magnetoacoustics in Nickel Films. *Phys. Rev. Lett.* **2012**, *109* (16), 166601.

(37) Berk, C.; Jaris, M.; Yang, W.; Dhuey, S.; Cabrini, S.; Schmidt, H. Strongly Coupled Magnon-Phonon Dynamics in a Single Nanomagnet. *Nat. Commun.* **2019**, *10*, 2652.

(38) Deb, M.; Popova, E.; Hehn, M.; Keller, N.; Mangin, S.; Malinowski, G. Picosecond Acoustic-Excitation-Driven Ultrafast Magnetization Dynamics in Dielectric Bi-Substituted Yttrium Iron Garnet. *Phys. Rev. B: Condens. Matter Mater. Phys.* **2018**, *98* (17), 174407.

(39) Kovalenko, O.; Pezeril, T.; Temnov, V. V. New Concept for Magnetization Switching by Ultrafast Acoustic Pulses. *Phys. Rev. Lett.* **2013**, *110* (26), 266602.

(40) Jäger, J. V.; Scherbakov, A. V.; Glavin, B. A.; Salasyuk, A. S.; Campion, R. P.; Rushforth, A. W.; Yakovlev, D. R.; Akimov, A. V.; Bayer, M. Resonant Driving of Magnetization Precession in a Ferromagnetic Layer by Coherent Monochromatic Phonons. *Phys. Rev. B: Condens. Matter Mater. Phys.* **2015**, *92* (2), 020404.

(41) Zhang, D.-L.; Zhu, J.; Qu, T.; Lattery, D. M.; Victora, R. H.; Wang, X.; Wang, J.-P. High-Frequency Magnetoacoustic Resonance Through Stain-Spin Coupling in Perpendicular Magnetic Multilayers. *Sci. Adv.* **2020**, *6* (38), No. eabb4607.

(42) Hashimoto, S.; Ochiai, Y.; Aso, K. Perpendicular Magnetic Anisotropy and Magnetostriction of Sputtered Co/Pd and Co/Pt Multilayered Films. *J. Appl. Phys.* **1989**, *66* (10), 4909−4916.

(43) Schelp, L. F.; Viegas, A. D. C.; Carara, M.; Schmidt, J. E. Magnetostriction of Co/Pd Multilayers. *J. Magn. Magn. Mater.* **1995**, *139*, 59−64.

(44) Parkin, S. S. P.; More, N.; Roche, K. P. Oscillations in Exchange Coupling and Magnetoresistance in Metallic Superlattice Structures: Co/Ru, Co/Cr, and Fe/Cr. *Phys. Rev. Lett.* **1990**, *64* (19), 2304−2307.

(45) Bruno, P. Theory of Interlayer Magnetic Coupling. *Phys. Rev. B: Condens. Matter Mater. Phys.* **1995**, *52* (1), 411−439.

(46) Bandiera, S.; Sousa, R. C.; Dahmane, Y.; Ducruet, C.; Portemont, C.; Baltz, V.; Auffret, S.; Prejbeanu, I. L.; Dieny, B. Comparison of Synthetic Antiferromagnets and Hard Ferromagnets as Reference Layer in Magnetic Tunnel Junctions With Perpendicular Magnetic Anisotropy. *IEEE Magn. Lett.* **2010**, *1*, 3000204.

(47) You, C. Y. Effect of the Synthetic Antiferromagnetic Polarizer Layer Rigidness on the Spin Transfer Torque Switching Current Density. *Appl. Phys. Lett.* **2013**, *103* (4), 042402.

(48) Zhang, D. L.; Sun, C.; Lv, Y.; Schliep, K. B.; Zhao, Z.; Chen, J. Y.; Voyles, P. M.; Wang, J. P. L1$_0$ Fe-Pd Synthetic Antiferromagnet Through an fcc Ru Spacer Utilized for Perpendicular Magnetic Tunnel Junctions. *Phys. Rev. Appl.* **2018**, *9* (4), 044028.

(49) Houssameddine, D.; Sierra, J. F.; Gusakova, D.; Delaet, B.; Ebels, U.; Buda-Prejbeanu, L. D.; Cyrille, M. C.; Dieny, B.; Ocker, B.; Langer, J.; Maas, W. Spin Torque Driven Excitations in a Synthetic Antiferromagnet. *Appl. Phys. Lett.* **2010**, *96* (7), 072511.

(50) Duine, R. A.; Lee, K.-J.; Parkin, S. S. P.; Stiles, M. D. Synthetic Antiferromagnetic Spintronics. *Nat. Phys.* **2018**, *14* (3), 217−219.

(51) Yang, H.; Li, Y.; Bailey, W. E. Large Spin Pumping Effect in Antisymmetric Precession of $Ni_{79}Fe_{21}/Ru/Ni_{79}Fe_{21}$. *Appl. Phys. Lett.* **2016**, *108* (24), 242404.

(52) Tanaka, K.; Moriyama, T.; Nagata, M.; Seki, T.; Takanashi, K.; Takahashi, S.; Ono, T. Linewidth Broadening of Optical Precession Mode in Synthetic Antiferromagnet. *Appl. Phys. Express* **2014**, *7*, 063010.

(53) Sorokin, S.; Gallardo, R. A.; Fowley, C.; Lenz, K.; Titova, A.; Atcheson, G. Y. P.; Dennehy, G.; Rode, K.; Fassbender, J.; Lindner, J.; Deac, A. M. Magnetization Dynamics in Synthetic Antiferromagnets: Role of Dynamical Energy and Mutual Spin Pumping. *Phys. Rev. B: Condens. Matter Mater. Phys.* **2020**, *101* (14), 144410.

(54) Kamimaki, A.; Iihama, S.; Taniguchi, T.; Mizukami, S. All-Optical Detection and Evaluation of Magnetic Damping in Synthetic Antiferromagnet. *Appl. Phys. Lett.* **2019**, *115* (13), 132402.

(55) Wu, G.; Chen, S.; Ren, Y.; Jin, Q. Y.; Zhang, Z. Laser-Induced Magnetization Dynamics in Interlayer-Coupled $[Ni/Co]_4/Ru/[Co/Ni]_3$ Perpendicular Magnetic Films for Information Storage. *ACS Appl. Nano Mater.* **2019**, *2* (8), 5140−5148.

(56) Wu, G.; Chen, S.; Lou, S.; Liu, Y.; Jin, Q. Y.; Zhang, Z. Annealing Effect on Laser-Induced Magnetization Dynamics in Co/Ni-Based Synthetic Antiferromagnets With Perpendicular Magnetic Anisotropy. *Appl. Phys. Lett.* **2019**, *115* (14), 142402.

(57) Mizukami, S.; Wu, F.; Sakuma, A.; Walowski, J.; Watanabe, D.; Kubota, T.; Zhang, X.; Naganuma, H.; Oogane, M.; Ando, Y.; Miyazaki, T. Long-Lived Ultrafast Spin Precession in Manganese Alloys Films With a Large Perpendicular Magnetic Anisotropy. *Phys. Rev. Lett.* **2011**, *106* (11), 117201.

(58) Mekonnen, A.; Cormier, M.; Kimel, A. V.; Kirilyuk, A.; Hrabec, A.; Ranno, L.; Rasing, T. Femtosecond Laser Excitation of Spin Resonances in Amorphous Ferrimagnetic $Gd_{1-x}Co_x$ Alloys. *Phys. Rev. Lett.* **2011**, *107* (11), 117202.

(59) Zhang, Z.; Zhou, L.; Wigen, P. E.; Ounadjela, K. Angular Dependence of Ferromagnetic Resonance in Exchange-Coupled Co/Ru/Co Trilayer Structures. *Phys. Rev. B: Condens. Matter Mater. Phys.* **1994**, *50* (9), 6094−6112.

(60) Mandal, R.; Ogawa, D.; Tamazawa, Y.; Ishioka, K.; Shima, T.; Kato, T.; Iwata, S.; Takahashi, Y. K.; Hirosawa, S.; Hono, K. Time Domain Magnetization Dynamics Study to Estimate Interlayer Exchange Coupling Constant in Nd-Fe-B/$Ni_{80}Fe_{20}$ Films. *J. Magn. Magn. Mater.* **2018**, *468*, 273−278.

(61) Mondal, S.; Choudhury, S.; Jha, N.; Ganguly, A.; Sinha, J.; Barman, A. All-Optical Detection of the Spin Hall Angle in W/$CoFeB/SiO_2$ Heterostructures With Varying Thickness of the Tungsten Layer. *Phys. Rev. B: Condens. Matter Mater. Phys.* **2017**, *96* (5), 054414.

(62) Panda, S. N.; Mondal, S.; Sinha, J.; Choudhury, S.; Barman, A. All-Optical Detection of Interfacial Spin Transparency From Spin Pumping in,-Ta/CoFeB Thin Films. *Sci. Adv.* **2019**, *5* (4), No. eaav7200.

(63) Chumak, A. V.; Serga, A. A.; Hillebrands, B. Magnon Transistor for All-Magnon Data Processing. *Nat. Commun.* **2014**, *5*, 4700.

(64) Iihama, S.; Sasaki, Y.; Sugihara, A.; Kamimaki, A.; Ando, Y.; Mizukami, S. Quantification of a Propagating Spin-Wave Packet Created by an Ultrashort Laser Pulse in a Thin Film of a Magnetic Metal. *Phys. Rev. B: Condens. Matter Mater. Phys.* **2016**, *94* (2), 020401.

(65) Zhu, J.; Park, H.; Chen, J.-Y.; Gu, X.; Zhang, H.; Karthikeyan, S.; Wendel, N.; Campbell, S. A.; Dawber, M.; Du, X.; Li, M.; Wang, J.-P.; Yang, R.; Wang, X. Revealing the Origins of 3D Anisotropic Thermal Conductivities of Black Phosphorus. *Adv. Electron. Mater.* **2016**, *2* (5), 1600040.

(66) Chen, J.-Y.; Zhu, J.; Zhang, D.; Lattery, D. M.; Li, M.; Wang, J.-P.; Wang, X. Time-Resolved Magneto-Optical Kerr Effect of Magnetic Thin Films for Ultrafast Thermal Characterization. *J. Phys. Chem. Lett.* **2016**, *7* (13), 2328−2332.

(67) Feser, J. P.; Liu, J.; Cahill, D. G. Pump-Probe Measurements of the Thermal Conductivity Tensor for Materials Lacking in-Plane Symmetry. *Rev. Sci. Instrum.* **2014**, *85* (10), 104903.

(68) Liu, J.; Choi, G.-M.; Cahill, D. G. Measurement of the Anisotropic Thermal Conductivity of Molybdenum Disulfide by the Time-Resolved Magneto-Optic Kerr Effect. *J. Appl. Phys.* **2014**, *116* (23), 233107.

(69) Koopmans, B.; Malinowski, G.; Dalla Longa, F.; Steiauf, D.; Fähnle, M.; Roth, T.; Cinchetti, M.; Aeschlimann, M. Explaining the Paradoxical Diversity of Ultrafast Laser-Induced Demagnetization. *Nat. Mater.* **2010**, *9*, 259−265.

(70) Choi, G.-M.; Min, B.-C.; Lee, K.-J.; Cahill, D. G. Spin Current Generated by Thermally Driven Ultrafast Demagnetization. *Nat. Commun.* **2014**, *5*, 4334.